Editors' Suggestion

Highly Efficient Single-Exciton Strong Coupling with Plasmons by Lowering Critical Interaction Strength at an Exceptional Point

Wei Li,[1,3] Renming Liu,[2,*] Junyu Li,[1] Jie Zhong,[1] Yu-Wei Lu,[1] Huanjun Chen,[3] and Xue-Hua Wang[1,†]

[1]State Key Laboratory of Optoelectronic Materials and Technologies, School of Physics, Sun Yat-sen University, Guangzhou 510275, China

[2]School of Physics and Electronics, International Joint Research Laboratory of New Energy Materials and Devices of Henan Province, Henan University, Kaifeng 475004, China

[3]School of Electronics and Information Technology, Sun Yat-sen University, Guangzhou 510006, China

(Received 1 March 2022; accepted 24 February 2023; published 5 April 2023)

The single-exciton strong coupling with the localized plasmon mode (LPM) at room temperature is highly desirable for exploiting quantum technology. However, its realization has been a very low probability event due to the harsh critical conditions, severely compromising its application. Here, we present a highly efficient approach for achieving such a strong coupling by reducing the critical interaction strength at the exceptional point based upon the damping inhibition and matching of the coupled system, instead of enhancing the coupling strength to overcome the system's large damping. Experimentally, we compress the LPM's damping linewidth from about 45 nm to about 14 nm using a leaky Fabry–Perot cavity, a good match to the excitonic linewidth of about 10 nm. This method dramatically relaxes the harsh requirement in mode volume by more than an order of magnitude and allows a maximum direction angle of the exciton dipole relative to the mode field of up to around 71.9°, significantly improving the success rate of achieving the single-exciton strong coupling with LPMs from about 1% to about 80%.

DOI: 10.1103/PhysRevLett.130.143601

Strong light-matter interactions have been a central topic in quantum optics and nanophotonics, showing various applications in quantum technologies such as quantum logic gates [1], single-atom lasers [2], and quantum information processing [3–6], which rely on a single quantum emitter (a two-level atom, molecule, or exciton) strongly interacting with a single-mode field via the coherent exchange of energy between the components of light and matter [7,8]. Under this condition, light and matter lose their separate identities and assume new mixed states, which significantly modulate the optical response of the system to external stimuli depending on the coupling strength [9]. For achieving such a single-emitter strong coupling, it is believed that the coupling strength between the two subsystems must exceed their respective dissipations [10–12].

Generally, there are two ways to realize a single-emitter strong coupling with electromagnetic modes. One way is to make the damping of the two subsystems very low, such as in the traditional atomic [13,14] and solid-state microcavity systems [7,15–17] operated at cryogenic temperature and in ultrahigh vacuum. The other is to greatly enhance the coupling strength of the coupled system for overcoming large dissipations at room temperature, such as the plasmonic nanocavity systems coupled with quantum emitters. In the past two decades, this emerging field has made great progress by squeezing the mode volume (V_m) of the localized plasmon modes (LPMs) to greatly improve the coupling strength [18–28]. Although impressive experiments have successfully demonstrated the room-temperature strong coupling between a few quantum emitters and the LPMs with ultrasmall V_m [26–32], realizing such single-emitter strong coupling remains a random event with low possibility, around 1% [29,33], due to the severe requirements for both the ultrasmall V_m and direction aligning of the emitter's dipole moment with the LPM field. These challenges in the room-temperature strong coupling field stem from large damping of the plasmon modes. In this Letter, we propose a strategy to significantly relax these harsh requirements by suppressing the damping of the LPM via a leaky Fabry-Perot (FP) cavity for a good match to the excitonic damping, which greatly improves the success rate of achieving the room-temperature strong coupling of a single exciton with a LPM from 1% to about 80%. This method further advance room-temperature quantum devices.

The LPM-exciton coupled system can be described by the following effective non-Hermitian Hamiltonian [34]

$$H_{\mathrm{eff}} = (\varepsilon_d - i\Gamma_d/2)d^+d + (\varepsilon_c - i\Gamma_c/2)c^+c + g(d^+c + c^+d), \quad (1)$$

where $\varepsilon_d(\varepsilon_c)$ and $\Gamma_d(\Gamma_c)$ are the energy and damping linewidth of the LPM (exciton); d and c (d^+ and c^+) are the annihilation (creation) operators for the LPM and exciton,

respectively; and g is the coupling strength between a single exciton and the LPM. The eigenlevels ($E_{\pm}^{l}$) of the hybrid system can be obtained as [8,28,35]

$$E_{\pm}^{l} = (\varepsilon_d + \varepsilon_c)/2 - i(\Gamma_d + \Gamma_c)/4 \pm \Omega_{\mathrm{LS}}/2, \quad (2)$$

with the level splitting (LS) of $\Omega_{\mathrm{LS}} = 2\sqrt{g^2 - [(\Gamma_d - \Gamma_c)/4 + i\delta/2]^2}$, where $\delta = \varepsilon_d - \varepsilon_c$ is the detuning between the two coupling components. At resonance ($\delta = 0$), the LS is expressed as

$$\Omega_{\mathrm{LS}} = 2\sqrt{g^2 - g_{\mathrm{EP}}^2} \quad \text{if } g^2 > g_{\mathrm{EP}}^2 = (\Gamma_d - \Gamma_c)^2/16, \quad (3)$$

where $g_{\mathrm{EP}} = |\Gamma_d - \Gamma_c|/4$ is the critical interaction strength at the exceptional point (EP). When $g = g_{\mathrm{EP}}$, the non-Hermitian coupled system is at the EP where the eigenlevels and the eigenstates are simultaneously coalesced (Sec. S1 [36]) [50,51]. Recently, research on the EPs and their associated applications has become an emerging field with intense activities [52–55]. Theoretically, as shown in Fig. S1(a) [36], when $g < g_{\mathrm{EP}}$, the system is in the weak coupling regime without the LS. When $g > g_{\mathrm{EP}}$, the eigen level splits into two branches [56], which is the precondition for strong coupling. Therefore, the lower the g_{EP}, the larger the Ω_{LS}, and achieving the single-exciton strong coupling becomes a possibility.

Experimentally, the LS of strong coupling systems is usually probed by the spectral Rabi splitting (SRS) in either absorption or emission based on the equality assumption of the SRS and LS, which causes controversy over the critical criteria of the strong coupling due to the invalidity of the equality assumption. Our recent work has addressed this issue [34] and revealed the relativity and diversity of the strong coupling (Fig. S2 in Sec. S2 [36]). For the coupling systems of a single exciton with the LPM, the absorption SRS ($\Omega_{\mathrm{SRS}}^{\mathrm{ab}}$) and its critical criterion are dominated by the plasmon channel signal [34],

$$\Omega_{\mathrm{SRS}}^{\mathrm{ab}} = 2\sqrt{g(1 + \Gamma_c/\Gamma_d)\cdot(g^2 + \Gamma_c\Gamma_d/4)^{1/2} - (g^2 + \Gamma_c\Gamma_d/4)\cdot\Gamma_c/\Gamma_d} \quad \text{if } g^2 > (g_{\mathrm{SRS}}^{\mathrm{ab}})^2 = \frac{\Gamma_c^2}{8(1 + \Gamma_d/2\Gamma_c)}. \quad (4)$$

We refer to this condition as the absorption strong coupling criterion. Additionally, the emission SRS requires that the LS of the coupled system is larger than the damping linewidth of the levels, i.e., $\Omega_{\mathrm{LS}} > (\Gamma_d + \Gamma_c)/2$, giving the emission SRS ($\Omega_{\mathrm{SRS}}^{\mathrm{em}}$) and its critical criterion as [57]

$$\Omega_{\mathrm{SRS}}^{\mathrm{em}} = 2\sqrt{g^2 - (g_{\mathrm{SRS}}^{\mathrm{em}})^2} \quad \text{if } g^2 > (g_{\mathrm{SRS}}^{\mathrm{em}})^2 = (\Gamma_d^2 + \Gamma_c^2)/8, \quad (5)$$

which is referred to as the emission strong-coupling criterion.

Evidently, the critical criteria of the LS, absorption, and emission SRS are different. From Eqs. (4) and (5) we find that $g_{\mathrm{SRS}}^{\mathrm{em}} > g_{\mathrm{SRS}}^{\mathrm{ab}}$ and $g_{\mathrm{SRS}}^{\mathrm{em}} > g_{\mathrm{EP}}$ are always fulfilled if $\Gamma_d > \Gamma_c$, which implies the realization of emission strong coupling is more difficult than the absorption and LS strong couplings. Importantly, we find from Eqs. (3) and (5) that if the plasmonic linewidth Γ_d can be sufficiently compressed to match it with the excitonic linewidth Γ_c, the critical interaction strength g_{EP} will be significantly reduced, even down to zero, and the Ω_{LS} will correspondingly be enlarged up to $2g$. Simultaneously, the emission strong-coupling condition is also remarkably lowered. Therefore, suppressing the plasmonic damping provides an effective way to easily realize and observe the single-exciton strong coupling with plasmons.

It is known that the plasmon mode can be engineered by the surrounding electromagnetic environment provided by optical microcavities, generating hybrid plasmonic-photonic modes with small V_m and moderate Q factors [58–61]. Here, we utilize a leaky FP cavity to suppress the damping of the LPM. When the LPM supported by a metal nanoparticle is resonant to the cavity modes, the LPM can be significantly sculpted by these modes due to the coupling between them [Fig. 1(a)]. The degree of the linewidth suppression is mainly dictated by the quality factor of the cavity mode and the coupling strength between the cavity mode and the LPM. The mechanism of the damping suppression of the LPM is discussed in detail based on an analytical quantum model in Sec. S3.1 [36] and further demonstrated by numerical simulations in Sec. S3.2 [36]. Next, we experimentally demonstrate that this approach works very well.

Figure 1(b) shows the reflection spectrum of the leaky FP cavity constructed by three dielectric layers of $Si/SiO_2/Si_3N_4$ (Fig. S7 in Sec. S4 [36]), showing three discrete leaky FP-cavity modes of TM1 $\sim$ 588 nm, TM2 $\sim$ 627 nm, and TM3 $\sim$ 670 nm in the region of 575–700 nm. It is found that the measurement is consistent with our simulated result by the finite element method (FEM) based on the structural parameters extracted from measurements. Figure 1(c) gives the typical dark-field scattering spectra of three cavity-engineered Au (core)-Ag (shell) (Au@Ag) nanorods (NRs) with aspect ratios of about 1.83, 2.12, and 2.23. The light scattering of the three cavity-engineered Au@Ag NRs reaches the maxima near the cavity modes of TM1, TM2, and TM3,

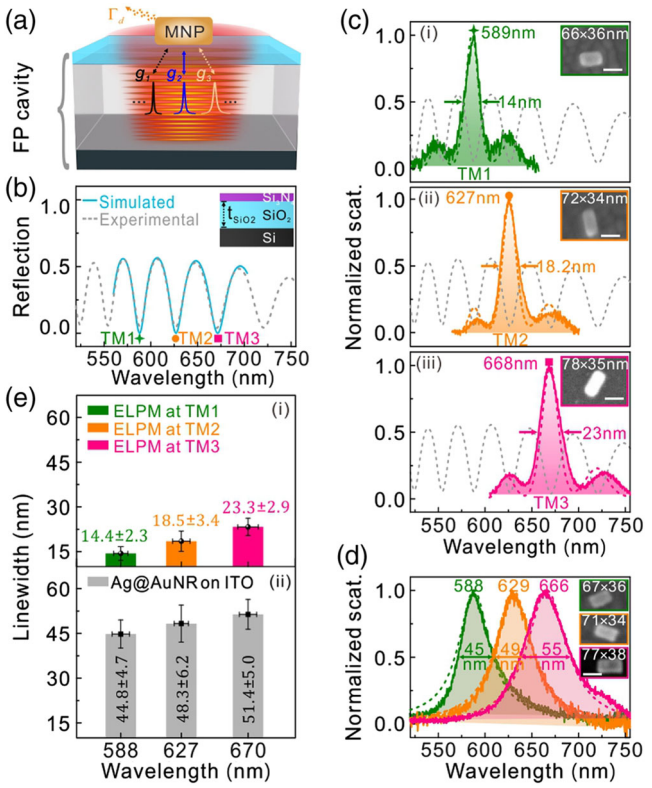

FIG. 1. (a) Schematics of a metal nanoparticle (MNP) residing in the microcavity-engineered electromagnetic environment. Here, g_k is the coupling strength between the dipolar LPM and the kth FP-cavity mode ($k = 1, 2, 3\ldots$). (b) Simulated and measured reflectance for the leaky FP cavity with $t_{Si_3N_4} = 216.9$ nm and $t_{SiO_2} = 3008$ nm. (c),(d) Normalized scattering (solid colored curves) of the Au@Ag NRs located on (c) the FP cavity and (d) the ITO-coated glass substrate, respectively. The dashed colored curves are simulated results using FEM based on the structural parameters extracted from the measurements. The dashed gray curves represent the experimental reflectance of the bare FP cavity. The inserts are SEM images for the measured Au@Ag NRs; the scale bar is 50 nm. (e) Statistics of damping linewidths of the ELPMs for the Au@Ag NRs localized on the FP cavity (balls) and the LPMs for the NRs on the ITO substrate (squares). Note that the counted range of the ELPM's and LPM's wavelengths centered around the cavity modes of 588, 627, and 670 nm in a range of ± 8 nm.

respectively. As we have predicted in Sec. S3 [36], when the LPM supported by the bare Au@Ag NR resonates with a FP-cavity mode, the LPM will be significantly sculpted and greatly enhanced by this mode. Because different FP-cavity modes possess different spectral bandwidths, the three new engineered LPMs (ELPMs) at about 589, 627, and 668 nm have different damping linewidths of around 14.0, 18.2, and 23.0 nm, respectively, indicating that the ELPM's damping linewidth can be flexibly harnessed by designing the bandwidth of the corresponding FP-cavity mode. Compared to the LPMs supported by the bare Au@Ag NRs [Fig. 1(d)] with resonance or near resonance to these cavity modes, the damping linewidths of the ELPMs are compressed to about 1/3 of their respective original LPMs [Fig. 1(c)]. Particularly, the damping linewidth of 14 nm for the ELPM at 589 nm matches well with that ($\Gamma_c = 10$ nm) of the J-aggregate exciton (Fig. S9 in Sec. S5 [36]), providing the possibility to greatly lower the g_{EP} of the plasmon-exciton coupling system. Figures 1(c) and 1(d) show good agreement between the measurements and the simulated results.

Notably, when the bare LPMs are sculpted by a given FP-cavity mode (for instance, TM1), the resonance frequencies and damping linewidths of the newly formed ELPM are in very close proximity to those of this cavity mode, with only small deviations (Fig. S10 [36]). The ELPM's frequency can also be tuned in a broader spectral region by varying the cavity length t_{SiO_2} of the leaky FP cavities (Fig. S11 [36]). Figure 1(e)(i) shows the statistics of the damping linewidths of 14.4 ± 2.3, 18.5 ± 3.4, and 23.3 ± 2.9 nm for the ELPMs (balls) around the cavity modes of TM1, TM2, and TM3, respectively. Compared to the statistical linewidths (44.8 ± 4.7, 48.3 ± 6.2, and 51.4 ± 5.0 nm) of the LPMs for the NRs fixed on indium tin oxide (ITO)-coated glass substrate [the squares in Fig. 1(e)(ii)], the damping linewidths of the ELPMs are remarkably suppressed.

To illuminate the effectiveness of our approach, we first demonstrate the challenges in achieving the strong coupling of a single exciton with an Au@Ag NR without FP-cavity engineering in Sec. S6 [36]. Although an ultrasmall mode volume of $V_m \sim 91$ nm^3 (Sec. S7.3 [36]) and a considerable coupling strength of $g \sim 29.7$ meV (Sec. S7.4 [36]) can be obtained in such a state-of-the-art hybrid system, the large plasmonic damping ($\Gamma_d \sim 159$ meV) and the remarkable damping mismatch with that of the exciton ($\Gamma_c \sim 36$ meV) induce a high critical interaction strength ($g_{EP} = 30.75$ meV) of the coupled system, which means that the LS condition of $g > g_{EP}$ cannot be satisfied even in the case showing an evident SRS of about 69 meV [Fig. S12(c) [36]]. Therefore, the coupled system is in a pseudo-strong-coupling regime [34].

To push the single-exciton coupling systems into the strong coupling regime, we locate the single-exciton-coupled NRs on top of the FP cavity to lower its g_{EP} and total damping. Then, the dark-field scattering measurements of the cavity-engineered coupled systems are performed, shown in Fig. 2(a). Figure 2(b) gives a typical scattering spectrum, showing a clear SRS of $\Omega_{SRS} \sim 63$ meV. The dashed pink curve in Fig. 2(b) is the theoretical spectrum calculated using Eq. (S11) (Sec. S6 [36]) with $N = 1$, $g = 30.87$ meV [extracted from Eq. (4) by fitting $\Omega_{SRS} = 63$ meV], $\Gamma_c = 36$ meV, and $\Gamma_d = 54$ meV [Fig. 2(c)], which shows a good consistency with the measurement. The matching of plasmonic and excitonic damping causes the g_{EP} of the coupled system to significantly decrease from 30.75 to 4.5 meV [Fig. 2(d)], giving

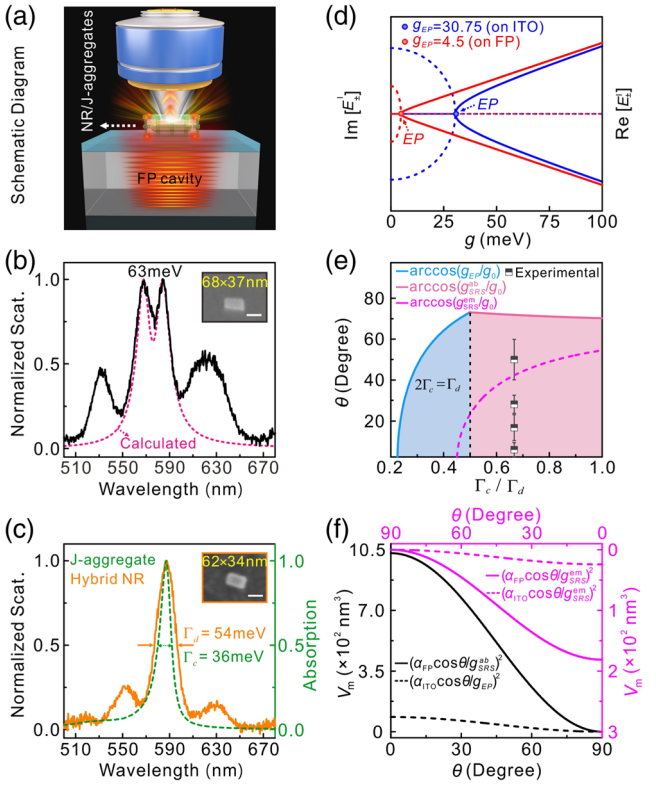

FIG. 2. (a) Schematic diagram of the dark-field measurement for an Au@Ag NR/J-aggregate hybrid on a leaky FP cavity. (b) Scattering spectrum of a single-exciton-coupled Au@Ag NR on the FP cavity. (c) Absorption spectra of the J-aggregate solution and the scattering spectrum of an Au@Ag NR located on the FP cavity. (d) Real (solid curves) and imaginary (dashed curves) parts of the eigenenergies in Eq. (2) as a function of g at resonance with $\Gamma_d = 159$ meV (on the ITO substrate) and $\Gamma_d = 54$ meV (on the FP cavity). (e) Maximum direction angle $\theta_{\max}$ as a function of Γ_c/Γ_d at absorption and emission strong coupling critical criteria, shown as colored solid and dashed curves. The squares are the estimated θ from the measured SRSs of individual single-exciton-coupled Au@Ag NRs on the FP cavity. (f) Under strong-coupling critical criteria, the allowed maximum V_m of the Au@Ag NRs with and without the cavity engineered at different θ.

rise to a dramatic increase of the Ω_{LS} from 0 to 59.1 meV. Furthermore, we also obtain $g_{\mathrm{SRS}}^{\mathrm{ab}} = 9.62$ meV and $g_{\mathrm{SRS}}^{\mathrm{em}} = 22.95$ meV; thus, the LS, absorption, and emission strong-coupling conditions can all be adequately satisfied at $g = 30.87$ meV.

The suppression of plasmonic damping lowers the critical criteria for realizing the single-exciton strong coupling, which greatly relaxes the harsh requirements for the direction angle θ of the excitonic dipole relative to the maximum electric field and the V_m of the plasmonic mode. The solid colored curves in Fig. 2(e) show the maximum direction angle $\theta_{\max}$ under the condition $g(\theta < \theta_{\max}) > \max\{g_{\mathrm{SRS}}^{\mathrm{ab}}, g_{\mathrm{EP}}\}$, which is calculated using Eqs. (S32) and (S33) as a function of Γ_c/Γ_d (Sec. S8 [36]). In the calculations, we take $\Gamma_d = 54$ meV, $\Gamma_c = 36$ meV, and $g_0 = 31$ meV (obtained at $\theta = 0°$ and $V_m \sim 99$ nm^3, Table S1 [36]). The maximum direction angle is estimated up to $\theta_{\max} = 71.9°$, a very loose condition for achieving the single-exciton strong coupling observed in absorption. Moreover, even under the stricter emission strong-coupling condition, the $\theta_{\max}$ is allowed to be up to 42.3° (Sec. S8 [36]). The squares in Fig. 2(e) are statistical θ values extracted from the measured SRS of individual single-exciton-coupled NRs on the FP cavity, demonstrating an experimental $\theta_{\max}$ of 57.1°. Even at such a large direction angle, the single-exciton strong coupling can still be achieved. Notably, the measured SRSs in these individual cavity-engineered single-exciton-coupled NRs are mainly distributed in about 46–63.3 meV (i.e., $g \sim 22.7$–31 meV), indicating that even the stricter emission strong-coupling condition in Eq. (5) can be fulfilled.

Figure 2(f) shows the maximum V_m allowed for achieving the strong coupling in single-exciton-coupled NR with and without FP-cavity engineering. Under the single-exciton absorption strong-coupling criterion, the maximum V_m allowed for the cavity-engineered Au @Ag NR is 12.1 times larger than that for the NR localized on ITO substrate (Sec. S9 [36]). Even under the emission strong-coupling criterion, the allowed maximum V_m can also be improved 7.5 times, indicating that the strict requirement on sample fabrication has been largely relaxed. The relaxation of the harsh requirements on V_m and θ is anticipated to significantly improve the success rate of achieving the room-temperature single-exciton strong coupling with the LPM. In experiments, the statistical success rate of more than 200 measured samples was as high as about 80%, a value 80 times larger than that reported in the literature [29,33], which is highly desirable in practical applications.

Figure 3(a) depicts the dispersions of the mixed states extracted from the measured SRSs of individual cavity-engineered single-exciton-coupled NRs with different detunings. The typical scattering spectra ordered according to the ELPM energy and their corresponding theoretical reproductions can be found in Fig. S19 [36]. These spectra show two split peaks, resulting in the upper plexciton branch and lower plexciton branch with anticrossing behavior. The dispersions in Fig. 3(a) exhibit a pronounced SRS of $\Omega_{\mathrm{SRS}} \sim 63$ meV, agreeing well with the theoretical predictions calculated using Eq. (2) with $N = 1$, $g = 31$ meV, $\varepsilon_c = 2.145$ eV, $\Gamma_c = 36$ meV, and $\bar{\Gamma}_d = 55.4$ meV [Fig. S20(a) [36]]. Figure 3(b) depicts the discrete steps of the effective coupling strengths, $\sqrt{N}g$, extracted from the measured SRSs of individual cavity-engineered single-exciton-coupled NRs using Eq. (S25) [36]. The statistic average value, $\bar{g} = 30.8 \pm 2.3$ meV, for the single-exciton strong coupling is consistent with the theoretical prediction of $g_0 = 31$ meV, which satisfies both the emission and absorption strong-coupling conditions. These results indicate that we have achieved the single-exciton

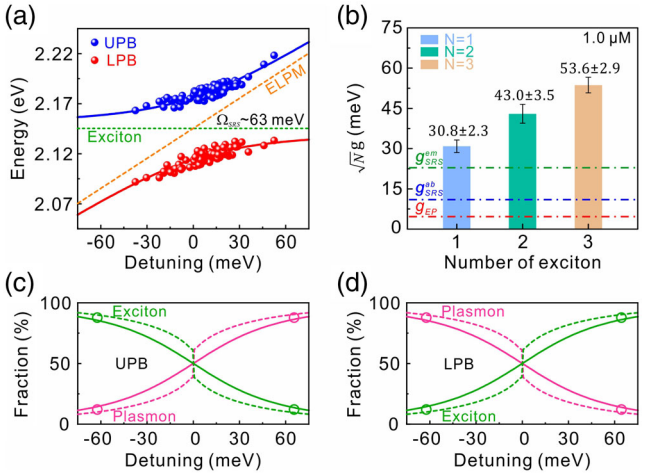

FIG. 3. (a) Energy dispersions of the mixed states extracted from the measurements (blue and red dots) and calculated (solid curves) using Eq. (2). Experimental ELPM energies were determined using laser-induced photobleaching technology (Sec. S10 [36]). (b) Discrete steps for effective coupling coefficient, $\sqrt{N}g$, extracted by fitting the observed SRSs with Eq. (S25) [36], corresponding to one, two, and three excitons involved in strong coupling, respectively. The dotted colored lines represent the critical conditions of LS, absorption, and emission strong coupling, calculated using Eqs. (3)–(5), respectively. (c),(d) Plasmonic and excitonic fractions in the (c) UPB and (d) LPB for the single-exciton-coupled NRs on the FP cavity (solid curves) and ITO substrate (dashed curves), respectively, which are calculated using Eq. (S2). In calculations for the samples located on the FP cavity, the parameters are the same as those used in Fig. 3(a), while, for the samples on the ITO substrate, the parameters are $N = 1$, $g = 29.7$ meV, $\Gamma_c = 36$ meV, and $\bar{\Gamma}_d = 158$ meV (Fig. S14 [36]). UPB: upper plexciton branch; LPB: lower plexciton branch.

strong coupling at room temperature in individual FP-cavity-engineered Au@Ag NRs. Importantly, about 80% of the measured samples can be assigned to the single-exciton strong coupling. However, about 20% of the measured samples are assigned to the multiexciton strong coupling [$N = 2$ or 3, Fig. 3(b)], Fano resonance, and spectrum broadening (Fig. S21 [36]), owing to the inevitable sample heterogeneity during the fabrication process. Additionally, we have also investigated the strong coupling of multi-excitons by increasing the dye concentration in the fabrication of Au@Ag NR/J-aggregate hybrids, and the mean values of the observed SRSs for such individual cavity-engineered multiexciton-coupled NRs are proportional to the square root of the dye concentration (Fig. S22 [36]). Figures 3(c) and 3(d) demonstrate the plasmonic and excitonic fractions in the upper and lower plexciton branches of the single-exciton-coupled NRs located on the ITO substrate and FP cavity, respectively. Interestingly, a steep variation in the fractions occurs at resonance ($\delta = 0$) for the hybrid samples measured on the ITO substrate, indicating that no level splitting occurs in such cases and the observed SRS is a pseudostrong coupling. Mixing fractions calculated for the coupling cases with much smaller g values can be found in Fig. S23 [36]. Compared to the samples measured on ITO, however, the plasmonic and excitonic fractions in the plexciton branches demonstrate a much clearer coherence characteristic in the cavity-engineered single-exciton-coupled NRs, owing to the significant suppression of plasmonic damping.

In summary, we have demonstrated that the large plasmon mode's damping, severely hindering plasmon nanophotonics' practical applications, can be effectively suppressed via a leaky FP cavity. A good damping match between the exciton and plasmon mode has been achieved through the plasmonic damping inhibition, which simultaneously lowers the critical interaction strength at the EP and total dissipative damping of the coupled system. Then, the level splitting is dramatically enlarged, and the critical strong-coupling criteria is reduced, which significantly relaxes the strict requirements (such as ultrasmall mode volume and dipole moment alignment) for achieving the single-exciton strong coupling with plasmons. These merits make the realization of room-temperature single-exciton strong coupling much more efficient, with a significantly improved success rate of up to around 80%. Our work further advances in room-temperature quantum devices based on single-qubit strong coupling.

This work was supported by the National Key R&D Program of China (Grant No. 2021YFA1400800), the National Natural Science Foundations of China (Grants No. 11874438 and No. 62205061), the Key-Area Research and Development Program of Guangdong Province (Grant No. 2018B030329001), and the Guangdong Special Support Program (Grant No. 2019JC05X397).

*liurm@henu.edu.cn
†wangxueh@mail.sysu.edu.cn

[1] T. G. Tiecke, J. D. Thompson, N. P. de Leon, L. R. Liu, V. Vuletic, and M. D. Lukin, Nature (London) **508**, 241 (2014).
[2] A. B. J. McKeever, A. D. Boozer, J. R. Buck, and H. J. Kimble, Nature (London) **425**, 268 (2003).
[3] A. Imamoğlu, D. D. Awschalom, G. Burkard, D. P. DiVincenzo, D. Loss, M. Sherwin, and A. Small, Phys. Rev. Lett. **83**, 4204 (1999).
[4] D. E. Chang, V. Vuletić, and M. D. Lukin, Nat. Photonics **8**, 685 (2014).
[5] G. Khitrova, H. M. Gibbs, M. Kira, S. W. Koch, and A. Scherer, Nat. Phys. **2**, 81 (2006).
[6] Z. C. Seskir and A. U. Aydinoglu, Int. J. Quantum. Inform. **19**, 2150012 (2021).
[7] K. Hennessy, A. Badolato, M. Winger, D. Gerace, M. Atatüre, S. Golde, S. Fält, E. L. Hu, and A. Imamoğlu, Nature (London) **445**, 896 (2007).
[8] P. Törmä and W. L. Barnes, Rep. Prog. Phys. **78**, 013901 (2015).

[9] H. Groß, J. M. Hamm, T. Tufarelli, O. Hess, and B. Hecht, Sci. Adv. **4**, eaar4906 (2018).
[10] K. J. Vahala, Nature (London) **424**, 839 (2003).
[11] O. Benson, Nature (London) **480**, 193 (2011).
[12] H. J. Kimble, Nature (London) **453**, 1023 (2008).
[13] T. Aoki, B. Dayan, E. Wilcut, W. P. Bowen, A. S. Parkins, T. J. Kippenberg, K. J. Vahala, and H. J. Kimble, Nature (London) **443**, 671 (2006).
[14] R. J. Thompson, G. Rempe, and H. J. Kimble, Phys. Rev. Lett. **68**, 1132 (1992).
[15] S. Groblacher, T. Paterek, R. Kaltenbaek, Č. Brukner, M. Żukowski, M. Aspelmeyer, and A. Zeilinger, Nature (London) **446**, 871 (2007).
[16] J. P. Reithmaier, G. Sęk, A. Löffler, C. Hofmann, S. Kuhn, S. Reitzenstein, L. V. Keldysh, V. D. Kulakovskii, T. L. Reinecke, and A. Forchel, Nature (London) **432**, 197 (2004).
[17] D. Englund, A. Faraon, I. Fushman, N. Stoltz, P. Petroff, and J. Vučković, Nature (London) **450**, 857 (2007).
[18] J. Bellessa, C. Bonnand, J. C. Plenet, and J. Mugnier, Phys. Rev. Lett. **93**, 036404 (2004).
[19] T. K. Hakala, J. J. Toppari, A. Kuzyk, M. Pettersson, H. Tikkanen, H. Kunttu, and P. Törmä, Phys. Rev. Lett. **103**, 053602 (2009).
[20] E. Waks and D. Sridharan, Phys. Rev. A **82**, 043845 (2010).
[21] D. E. Gomez, K. C. Vernon, P. Mulvaney, and T. J. Davis, Nano Lett. **10**, 274 (2010).
[22] S. Savasta, R. Saija, Alessandro Ridolfo, O. D. Stefano, P. Denti, and F. Borghese, ACS Nano **4**, 6369 (2010).
[23] A. E. Schlather, N. Large, A. S. Urban, P. Nordlander, and N. J. Halas, Nano Lett. **13**, 3281 (2013).
[24] G. Zengin, M. Wersäll, S. Nilsson, T. J. Antosiewicz, M. Käll, and T. Shegai, Phys. Rev. Lett. **114**, 157401 (2015).
[25] J. Ren, Y. Gu, D. Zhao, F. Zhang, T. Zhang, and Q. Gong, Phys. Rev. Lett. **118**, 073604 (2017).
[26] K. Santhosh, O. Bitton, L. Chuntonov, and G. Haran, Nat. Commun. **7**, ncomms11823 (2016).
[27] R. Chikkaraddy, B. de Nijs, F. Benz, S. J. Barrow, O. A. Scherman, E. Rosta, A. Demetriadou, P. Fox, O. Hess, and J. J. Baumberg, Nature (London) **535**, 127 (2016).
[28] R. Liu, Z.-K. Zhou, Y.-C. Yu, T. Zhang, H. Wang, G. Liu, Y. Wei, H. Chen, and X.-H. Wang, Phys. Rev. Lett. **118**, 237401 (2017).
[29] H. Leng, B. Szychowski, M. C. Daniel, and M. Pelton, Nat. Commun. **9**, 4012 (2018).
[30] H. Groß, J. M. Hamm, T. Tufarelli, O. Hess, and B. Hecht, Sci. Adv. **4**, eeav4906 (2018).
[31] K.-D. Park, M. A. May, H. Leng, J. Wang, J. A. Kropp, T. Gougousi, M. Pelton, and M. B. Raschke, Sci. Adv. **5**, eeav5931 (2019).
[32] J. Qin, Y.-H. Chen, Z. Zhang, Y. Zhang, R. J. Blaikie, B. Ding, and M. Qiu, Phys. Rev. Lett. **124**, 063902 (2020).
[33] J.-Y. Li, W. Li, J. Liu, J. Zhong, R. Liu, H. Chen, and X.-H. Wang, Nano Lett. **22**, 4686 (2022).
[34] R. Liu, Z. Liao, Y.-C. Yu, and X.-H. Wang, Phys. Rev. B **103**, 235430 (2021).
[35] T. Yoshie, A. Scherer, J. Hendrickson, G. Khitrova, H. M. Gibbs, G. Rupper, C. Ell, O. B. Shchekin, and D. G. Deppe, Nature (London) **432**, 200 (2004).
[36] See Supplemental Material at http://link.aps.org/supplemental/10.1103/PhysRevLett.130.143601 for detailed theory modeling, numerical calculations, experimental materials and methods, SEM, TEM images and dark-field scattering measurements of Au@Ag/J-aggregates, etc., including Figs. S1–S24, Tables S1, and Refs. [37–49].
[37] D. F. Walls and G. J. Milburn, *Quantum Optics* (Springer Science & Business Media, New York, 2007).
[38] G. González-Rubio, P. Díaz-Núñez, A. Rivera, A. Prada, G. Tardajos, J. González-Izquierdo, L. Bañares, P. Llombart, L. G. Macdowell, M. A. Palafox, L. M. Liz-Marzán, O. Peña-Rodríguez, and A. Guerrero-Martínez, Science **358**, 640 (2017).
[39] Y. Wang, J. Yu, Y.-F. Mao, J. Chen, S. Wang, H.-Z. Chen, Y. Zhang, S.-Y. Wang, X. Chen, T. Li, L. Zhou, R.-M. Ma, S. Zhu, W. Cai, and J. Zhu, Nature (London) **581**, 401 (2020).
[40] A. D. Rakić, A. B. Djurišić, J. M. Elazar, and M. L. Majewski, Appl. Opt. **37**, 5271 (1998).
[41] R. C. Hilborn, Am. J. Phys. **50**, 982 (1982).
[42] D. Melnikau, D. Savateeva, A. Chuvilin, R. Hillenbr, and Y. P. Rakovich, Opt. Express **19**, 22280 (2011).
[43] M. F. Limonov, M. V. Rybin, A. N. Poddubny, and Y. S. Kivshar, Nat. Photonics **11**, 543 (2017).
[44] A. Manjavacas, F. J. García de Abajo, and P. Nordlander, Nano Lett. **11**, 2318 (2011).
[45] D. N. Zubarev, Sov. Phys. Usp. **3**, 320 (1960).
[46] P. B. Johnson and R. W. Christy, Phys. Rev. B **6**, 4370 (1972).
[47] L. Novotny and B. Hecht, *Principle of Nano-Optics* (Cambridge University Press, Cambridge, 2006).
[48] R. Ruppin, Phys. Lett. A **299**, 309 (2002).
[49] C. Sauvan, J. P. Hugonin, I. S. Maksymov, and P. Lalanne, Phys. Rev. Lett. **110**, 237401 (2013).
[50] M.-A. Miri and A. Alú, Science **363**, eaar7709 (2019).
[51] Y.-W. Lu, J.-F. Liu, R. Liu, R. Su, and X.-H. Wang, Nanophotonics **10**, 2431 (2021).
[52] M. Naghiloo, M. Abbasi, Y. N. Joglekar, and K. W. Murch, Nat. Phys. **15**, 1232 (2019).
[53] Y. Wu, W. Liu, J. Geng, X. Song, X. Ye, C.-K. Duan, X. Rong, and J. Du, Science **364**, 878 (2019).
[54] F. Klauck, L. Teuber, M. Ornigotti, M. Heinrich, S. Scheel, and A. Szameit, Nat. Photonics **13**, 883 (2019).
[55] H.-Z. Chen, T. Liu, H.-Y. Luan, R.-J. Liu, X.-Y. Wang, X.-F. Zhu, Y.-B. Li, Z.-M. Gu, S.-J. Liang, H. Gao, L. Lu, L. Ge, S. Zhang, J. Zhu, and R.-M. Ma, Nat. Phys. **16**, 571 (2020).
[56] Y. Sang, C.-Y. Wang, S. S. Raja, C.-W. Cheng, C.-T. Huang, C.-A. Chen, X.-Q. Zhang, H. Ahn, C.-K. Shih, Y.-H. Lee, J. Shi, and S. Gwo, Nano Lett. **21**, 2596 (2021).
[57] G. Cui and M. G. Raymer, Phys. Rev. A **73**, 053807 (2006).
[58] H. M. Doeleman, E. Verhagen, and A. F. Koenderink, ACS Photonics **3**, 1943 (2016).
[59] Y. Yin, S. Li, S. Böttner, F. Yuan, S. Giudicatti, E. Saei Ghareh Naz, L. Ma, and O. G. Schmidt, Phys. Rev. Lett. **116**, 253904 (2016).
[60] P. Peng, Y.-C. Liu, D. Xu, Q.-T. Cao, G. Lu, Q. Gong, and Y.-F. Xiao, Phys. Rev. Lett. **119**, 233901 (2017).
[61] P. Wang, Y. Wang, Z. Yang, X. Guo, X. Lin, X.-C. Yu, Y.-F. Xiao, W. Fang, L. Zhang, G. Lu, Q. Gong, and L. Tong, Nano Lett. **15**, 7581 (2015).